Hindawi
Advances in Materials Science and Engineering
Volume 2021, Article ID 7925608, 16 pages
https://doi.org/10.1155/2021/7925608

Research Article

Influence of Confining Pressure Unloading Rate on the Strength Characteristics and Fracture Process of Granite Using Lab Tests

Jiaqi Guo,[1] Pengfei Liu,[1] Junqi Fan ,[2] Xiaoyan Shi,[2] and Xin Huang[1]

[1]*School of Civil Engineering, Henan Polytechnic University, Jiaozuo 454000, China*
[2]*Research Institute for National Defense Engineering of Academy of Military Science PLA China, Luoyang 471023, China*

Correspondence should be addressed to Junqi Fan; lyfjq@163.com

Received 13 April 2021; Accepted 29 May 2021; Published 16 July 2021

Academic Editor: Xianjie Hao

Copyright © 2021 Jiaqi Guo et al. This is an open access article distributed under the Creative Commons Attribution License, which permits unrestricted use, distribution, and reproduction in any medium, provided the original work is properly cited.

In order to study the mechanical behaviors and fracture process properties of granite under confining pressure unloading with constant axial pressure, RMT-150B rock mechanics test system and acoustic emission detector were used to study the mechanical properties and fracture process characteristics of deeply buried granite specimens under different combinations of initial confining pressures and unloading rates. The results show that when the unloading rate is small, the deviatoric stress-strain curve of granite specimens will yield an unloading platform, and the specimens show significant characteristics of ductility; when the unloading rate is large, the specimens show characteristics of brittleness. Besides, the axial strain rate increases with the increase of initial confining pressure and unloading rate, and the axial strain rate fluctuates. The ratio of axial strain increment to confining pressure increment of granite specimens decreases with the increase of the unloading rate, and a faster unloading rate and a higher initial confining pressure will restrain the axial deformation of granite sample. The normalized confining pressure decreased parameter of granite specimen increases with the increase of initial confining pressure. When the unloading rate is relatively high, it plays a dominant role in the compressive strength of granite specimens. The Mohr–Coulomb strength criterion can better reflect the strength characteristics of specimens under confining pressure unloading. The cohesion of granite specimens decreases with the increase of unloading rate, and the internal friction angle increases with the increase of unloading rate. Notably, the unloading rate presents a weakening effect on the cohesion of the specimen and a strengthening effect on the internal friction angle of the specimen, and the former effect is stronger than the latter one. When the unloading rate is small, the acoustic emission ringing count increases more evenly, and the deformation and damage of the specimen develop slowly; when the unloading rate is high, the acoustic emission ringing count increases to the maximum instantaneously at the initial stage of confining pressure unloading, and the specimen is damaged rapidly, showing the characteristic of sudden fracture. The fracture mode of granite specimens is affected by the unloading rate and initial confining pressure. At the same unloading rate, the specimens with high initial confining pressure show typical tensile fracture characteristics, while the specimens with low initial confining pressure mainly suffer from shear fracture or shear-tension composite fracture. With the increase of unloading rate, the fracture characteristics of specimens show a transition from shear or shear-tension composite fracture to tensile fracture.

1. Introduction

The excavation of underground engineering and the formation of cavern space have changed the spatial environment and initial stress state of rock mass, causing unloading of rock mass around the excavation area, and thus resulting in stress redistribution, stress concentration, and accumulation of a great number of elastic deformation properties in the surrounding rock. This provides space and dynamic conditions for the occurrence of underground engineering disasters, among which rock burst is a kind of common and extremely hazardous disaster [1–3]. Rock burst has a great impact and harm on the construction progress, construction cost, and personnel safety of underground engineering and has become a major safety hazard in underground engineering construction. Correct understanding of the unloading mechanical properties and fracture process law of the hard rock under confining pressure unloading is the

premise and foundation of revealing the mechanism of rock burst in underground engineering, accurately predicting and preventing rock burst and reasonably formulating prevention and control measures, which has important theoretical significance and application value [4–6].

A large number of underground engineering practices show that excavation unloading has a significant impact on the strength, deformation, and damage characteristics of hard rock [7–9]. Therefore, in recent years, scholars at home and abroad have conducted extensive and in-depth research on the mechanical properties of hard rock unloading. Xie H. Q et al. [10] found that rock specimens under confining pressure unloading mainly suffer from tensile fracture and shear fracture, and the brittleness of fracture is more obvious than that under the condition of loading. Li Hongzhe et al. [11] proposed that, under the same conditions, the decrement of confining pressure when unloading fracture occurs is significantly smaller than the increment of axial pressure when loading fracture occurs; that is, unloading is more likely to cause rock fracture. Li Jianlin et al.[12] found that the axial strain of sandstone specimens increases as the confining pressure unloading increases, showing a good exponential relationship between the two. Gao Feng et al. [13] obtained through laboratory tests that the peak strain of hard rock under confining pressure unloading is significantly reduced. Huang Runqiu et al. [14] held that, compared with the triaxial loading stress path, the internal friction angle of rock specimens under the unloading stress path increases, while the cohesion decreases significantly. Xuefeng Si et al. [15] found that under confining pressure unloading, the higher the initial confining pressure is, the more obvious the weakening effect of granite strength is. The above research results strongly promote the development of unloading rock mechanics, but the influence of unloading rate is not fully considered in the existing research, which, to a certain extent, affects the comprehensive understanding of unloading mechanical properties and fracture characteristics of hard rock [16–18].

In terms of the influence of unloading rate on mechanical properties and fracture characteristics of rock, Shili Qiu et al.[19, 20] studied the influence of unloading rate on rock strength and stated that rock strength increases with the increase of unloading rate. Huang Runqiu et al.[21] studied the deformation, fracture, and strength characteristics of marble of Jinping I Hydropower Station under different unloading rates in high-stress environment through indoor triaxial unloading test and SEM scanning analysis of fracture surface. Dai Bing et al. [22] carried out some triaxial tests with initial confining pressures of 10, 20, and 30 MPa and unloading rates of 0.05~1 MPa/s in three stress paths to investigate the deformation and dilation characteristics of rocks under different unloading rates of confining pressure. Wang Yunfei et al. [23] used rmt-150b rock mechanics test system to carry out stress path tests with constant axial pressure under confining pressure unloading and analyzed the strength, deformation, stability time, and damage fracture characteristics of white sandstone under confining pressure unloading. Peng Kang et al. [24] studied the fracture characteristics of granite under different unloading rates of confining pressure and considered that rock specimens are more prone to damage and fracture at high unloading rates of confining pressure. Research by Jiazhuo Li et al. [25] showed that under a slow unloading rate of confining pressure, more fracture surfaces are produced and the rock is broken more fully. Conversely, if the confining pressure is unloaded more quickly, the crack propagation and stress transfer are terminated abruptly and the rock specimen can only generate a few rupture surfaces along the initial rupture direction. It can be seen from the above research that the unloading rate of confining pressure has a significant impact on the mechanical properties and fracture characteristics of hard rock; but at present, there is still a long way to go for in-depth and systematic research on the deformation, strength, damage, and fracture characteristics of hard rock under different combinations of unloading rates and confining pressures [26–29].

In this study, using RMT-150B rock mechanics test system and acoustic emission detector, we carried out triaxial constant axial pressure tests under confining pressure unloading and acoustic emission monitoring under different unloading rates of confining pressure (0.002 MPa/s, 0.02 MPa/s, and 0.2 MPa/s) and different initial confining pressures (5 MPa, 10 MPa, and 20 MPa) for the deeply buried granite in Qinling mountainous area of Baoji City, Shaanxi Province. The ratio of axial strain increment to confining pressure increment $\Delta\varepsilon$, the rate of strain $\dot{\varepsilon}$, and the normalized confining pressure decreased parameter (k) were introduced, and the deformation and strength characteristics of granite under different combinations of unloading rates and initial confining pressures were analyzed. In addition, the applicability of the Mohr–Coulomb strength criterion in mechanics under confining pressure unloading was discussed. Based on the Mohr–Coulomb strength criterion, the variation law of the deformation parameters of granite specimens with the unloading rate of confining pressure was further studied. Meanwhile, according to the test results, the acoustic damage and fracture characteristics of hard rock were deeply and systematically studied under different combinations of unloading rates and initial confining pressures. The research results are of great significance to correctly understand the mechanical properties and damage characteristics of hard rock under confining pressure unloading, to accurately analyze the stability of surrounding rock with high energy storage, and to prevent rock burst disaster.

2. Experimental Investigations

2.1. Experimental Apparatus and Specimen Preparation. Triaxial confining pressure unloading tests were carried out by using the RMT-150B rock mechanics test system developed by the Institute of Rock and Soil Mechanics, Chinese Academy of Sciences (as shown in Figure 1). This test system can realize the real-time data acquisition of load, displacement, and other parameters during the test, with its maximum axial force being 1000 kN, the confining pressure being 50 MPa, and the frame stiffness of the testing machine being 5 GN/mm. Meanwhile, through the DS-5 8-channel

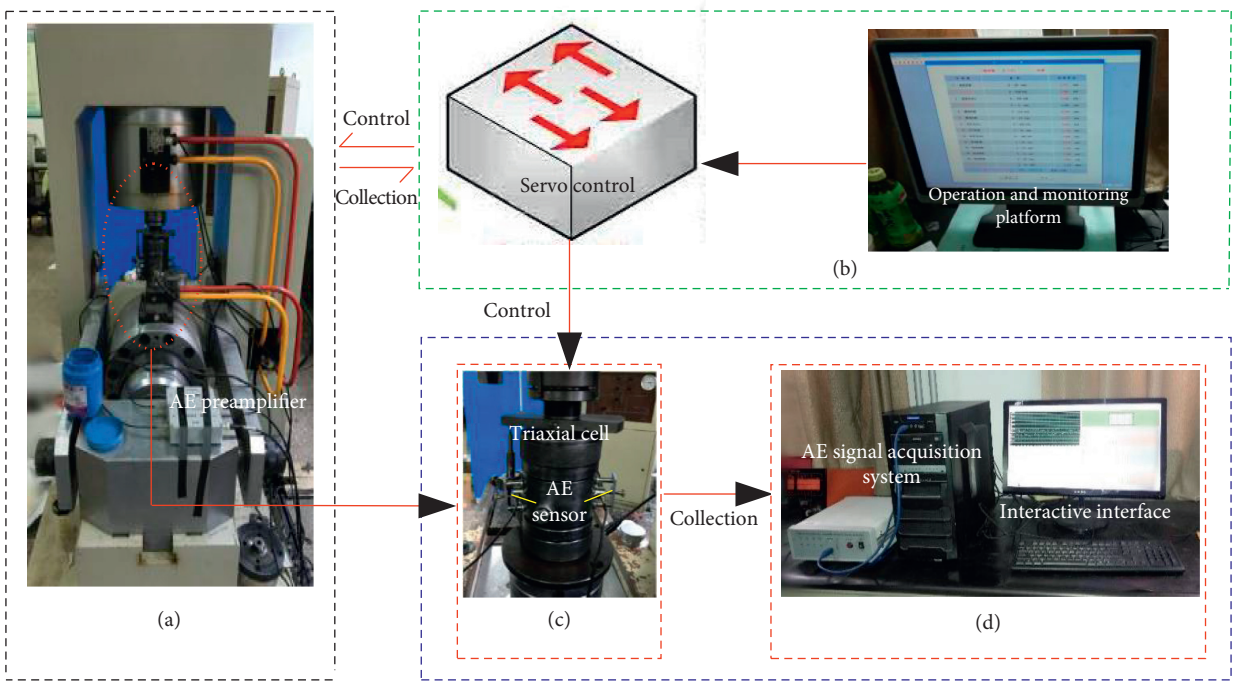

Figure 1: Experimental instruments. (a) RMT-150B rock mechanics test system. (b) Rock mechanics control system. (c) Main part of pressure chamber. (d) Acoustic emission synchronous detection system.

acoustic emission monitoring and analysis system, we can simultaneously monitor the AE amplitude, count, and energy of the specimens. The RS-2A acoustic emission sensor with a frequency of 150 kHz is arranged on both sides of the middle part of the specimen. The sensor and the specimen are coupled by a coupling agent and fixed by insulating tape. The sampling frequency of acoustic emission is set to 3 MHz, the threshold value is set to 50 dB, and the amplification factor is 40 dB.

The granite specimens used in this study are all taken from the buried depth of 560 meters of Tiantaishan Tunnel in Qinling Mountain, Baoji City, Shaanxi Province. The granite specimen is mainly composed of slightly weathered medium coarse-grained biotite granite. The rock is relatively hard, and the rock mass is relatively complete, with a smooth surface and no obvious defects. The sampling location is shown in Figures 2(a) and 2(b). In order to mitigate the discreteness of the test results, we drill in a large rock block to obtain the specimens. After drilling and coring, the specimens are put into the core box and transported to the laboratory. As shown in Figure 2(c), the specimen is cylindrical, about 50 mm in diameter, 100 mm in height, and 2.63 g/cm^3 in density. The machining accuracy of the specimen is strictly in accordance with the ISRM International Rock Mechanics Standard. The allowable deviation of end face roughness is ±0.05 mm. The end face should be perpendicular to the axis of the specimen, and the allowable deviation is ±0.25°.

2.2. Unloading Scheme. The initial damage, unloading path, and unloading rate are all important factors affecting the mechanical properties of granite under triaxial unloading. In order to analyze the effect of the unloading rate of confining pressure on the mechanical properties of granite, the initial damage and unloading path of confining pressure remain unchanged during the test. In this test, the initial damage degree of the granite specimen is set at 80% [19], which is achieved by adding axial pressure to 80% of conventional triaxial compressive strength under the corresponding confining pressure. As shown in Figure 3, the triaxial confining pressure unloading test often adopts three unloading paths: confining pressure unloading with constant axial pressure (O_1A), confining pressure unloading with increasing axial pressure (O_1B), and confining pressure unloading with decreasing axial pressure (O_1C). Among them, the triaxial test under confining pressure unloading with constant axial pressure (O_1A) can better simulate the unloading of surrounding rock after excavation in underground engineering, as well as the support situation that is not followed up in time [30, 31]. In addition, compared with other unloading paths, there are less stress variation factors when adopting the constant axial pressure unloading path; in other words, the specimen fracture is more directly induced by the confining pressure unloading. In this way, we can better analyze the deformation and fracture law of unloading rock mass with confining pressure unloading being the main influencing factor. Therefore, confining pressure unloading with constant axial pressure (O_1A) is adopted in this test (as shown in Figure 4).

This test adopts a stress path of confining pressure unloading with prepeak constant axial pressure. Firstly, confining pressure and axial pressure were applied to granite specimens at the loading rate of 0.05 MPa/s under

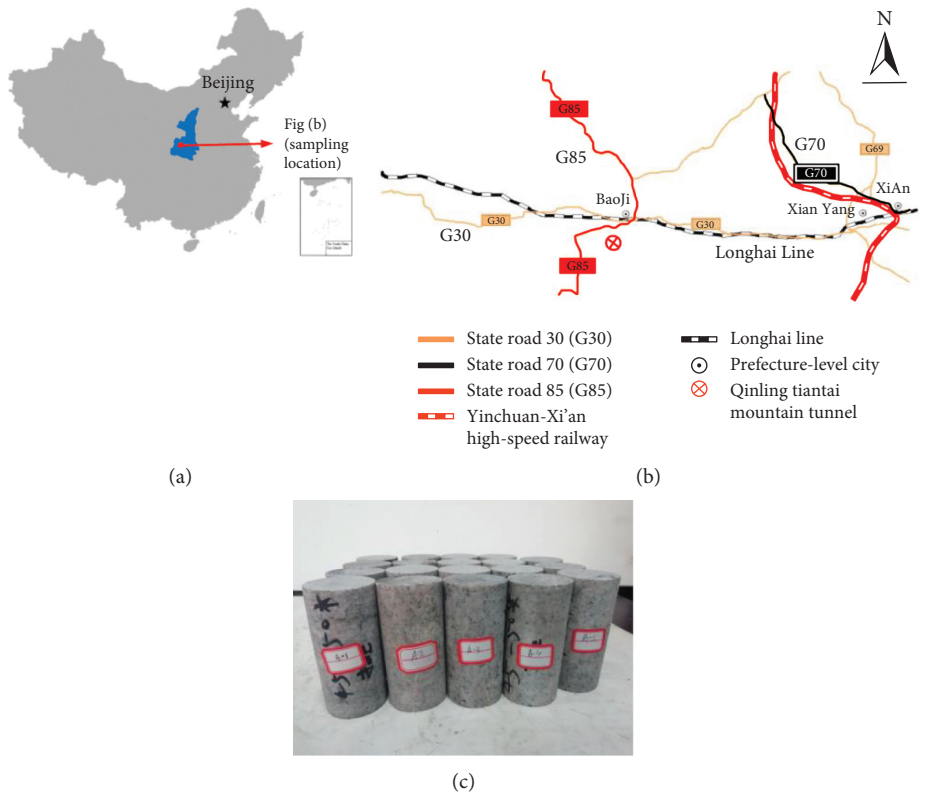

Figure 2: Granite rock samples and sampling location.

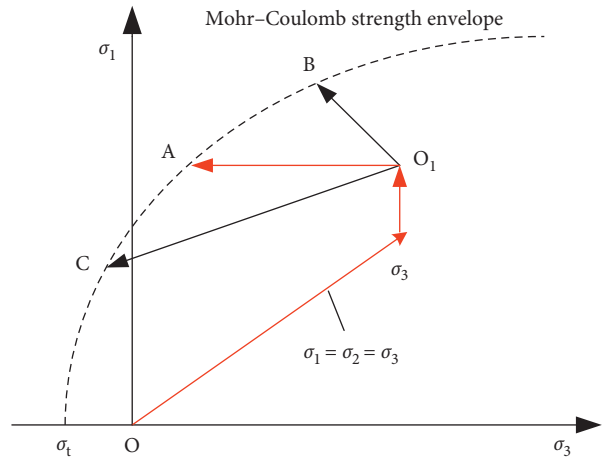

Figure 3: Schematic diagram of the stress of path in confining pressure unloading tests.

hydrostatic pressure to three predetermined stress levels of 5 MPa, 10 MPa, and 20 MPa. Then, at the loading rate of 1 kN/s, the axial load was applied continuously to the specimen until the load reached 80% of the conventional triaxial strength under the corresponding confining pressure (as shown in Table 1); afterward, the loading was stopped. It shall be noted that the confining pressure remained unchanged during the loading of axial pressure. Finally, the specimens were unloaded under confining pressure at the rates of 0.002 MPa/s, 0.02 MPa/s, and 0.2 MPa/s, respectively, with the axial pressure unchanged (as shown in Table 1), until the specimens were damaged. The test program automatically controlled the whole process, i.e., loading of confining pressure and axial pressure, and the unloading of confining pressure, which can ensure that the load is applied and removed to the preset values of the test. During the triaxial confining pressure unloading test, the acoustic emission test of granite specimens was carried out simultaneously.

3. Experimental Results and Analysis

3.1. Characteristics of Deviatoric Stress-Strain Curves under Different Unloading Rates and Confining Pressure. When the

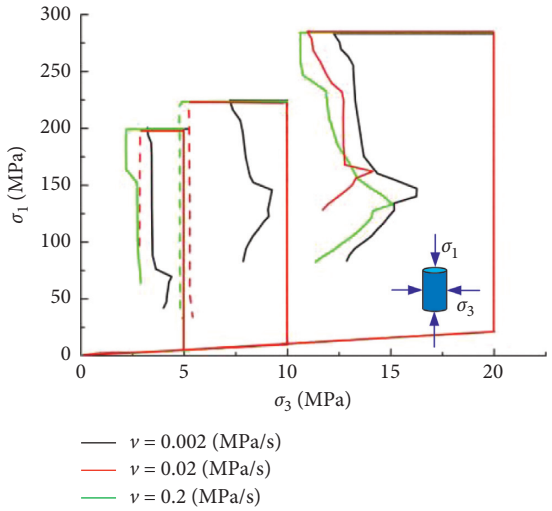

Figure 4: Relationship between σ_3 and σ_1 at different unloading confining pressure rates.

Table 1: Initial unloading state of rock sample.

Confining pressure unloading rate (MPa/s)	Initial confining pressure/MPa	Initial axial pressure/kN
0.2	5	369.98
	10	414.02
	20	529.96
0.02	5	370.04
	10	414.96
	20	529.84
0.002	5	369.98
	10	414.96
	20	529.96

confining pressure loaded onto the granite specimens is 5 MPa, 10 MPa, and 20 MPa, the deviatoric stress-strain relationship under conventional triaxial condition is shown in Figure 5(a); under different confining pressures, when the unloading rates of confining pressure are 0.002 MPa/s, 0.02 MPa/s, and 0.2 MPa/s, the deviatoric stress-strain relationship of the specimen is shown in Figures 5(b)–5(d), respectively.

It can be seen from Figure 5 that the deviatoric stress-strain curves of granite specimens all experienced four stages, i.e., the compaction stage, the linear elastic deformation stage, the plastic deformation stage, and the fracture stage, regardless of the conventional triaxial loading test or triaxial confining pressure unloading test with constant axial pressure. At the initial stage of loading, the original pores/cracks in the specimen are compacted, and the deviatoric stress-strain relationship shows obvious concave-down characteristics. With the continuous application of axial load, the specimen enters the stage of linear elastic deformation; that is, the higher the confining pressure is, the steeper the deviatoric stress-strain curve of the specimen is, and the greater the elastic modulus of the specimen is. In this stage, the granite specimens show obvious compressive hardening. At the end of the linear elastic deformation stage, the deviatoric stress-strain curve gradually becomes concave upward, the deformation of the specimen begins to enter the plastic stage, and the whole specimen presents elastic-plasticity. This study adopts the stress path of confining pressure unloading with constant axial pressure, the loading path of the specimens before confining pressure unloading is the same, and hence, the difference in the deviatoric stress-strain curves of the specimens is not significant.

According to Figures 5(b)–5(d), the deviatoric stress-strain curve of the granite specimen under confining pressure unloading is different from that under the conventional triaxial conditions. As shown in Figure 5(b), with a relatively large initial confining pressure and a relatively small unloading rate of confining pressure, although the deviatoric stress (σ_1-σ_3) of the specimen remains unchanged, the axial strain (ε_1) increases continuously, and the specimen shows obvious characteristics of axial plastic flow in the process of gradual confining pressure unloading. The results show that the deviatoric stress-strain curves of the specimens at different unloading rates of confining pressure have significant differences before and after the peak. Specifically, when the unloading rate of confining pressure is large, the specimen shows obvious brittleness; when the unloading rate of confining pressure is small, the deviatoric stress-strain curve of the specimen shows a section of approximately horizontal unloading platform before and after the peak, that is, the unloading effect is obvious, and the specimen shows obvious ductility.

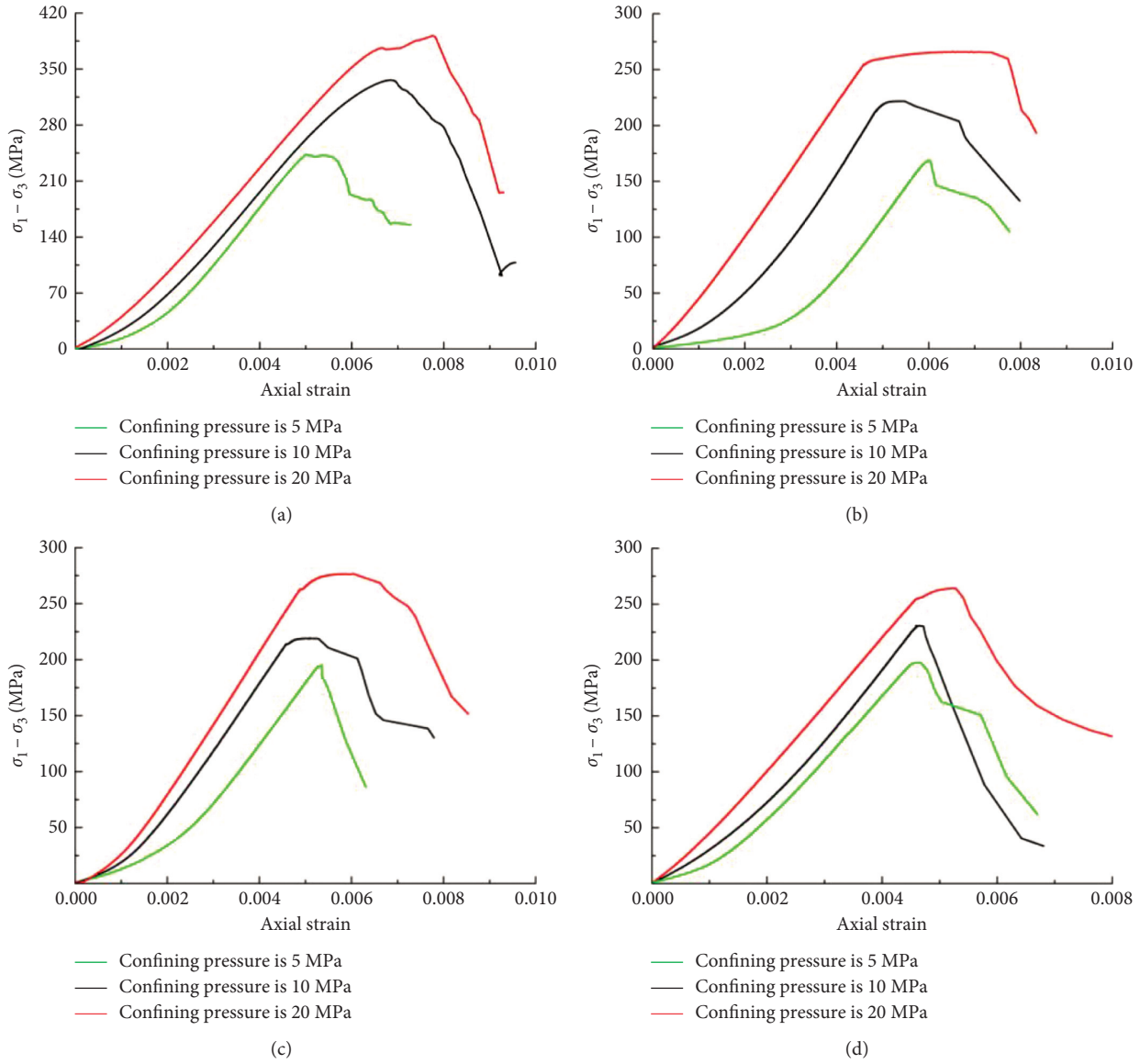

Figure 5: Deviatoric strain-stress curve of sandstone specimens under different confining pressure unloading rates. (a) Triaxial compression. (b) (v) = 0.002 MPa/s. (c) (v) = 0.02 MPa/s. (d) (v) = 0.2 MPa/s.

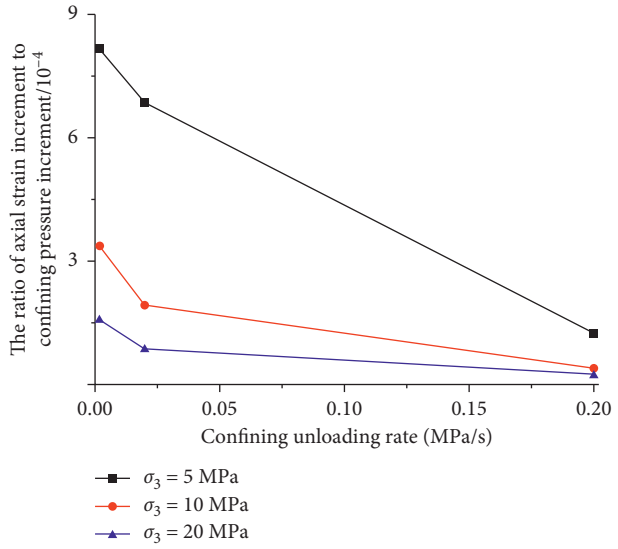

Figure 6: Relationships between $\Delta\varepsilon$ and unloading rates of confining pressure of granite.

3.2. Influence of Unloading Rate on the Deformation Characteristics of Granite Specimen. In the confining pressure unloading test, the strength, deformation, and other mechanical characteristics of the specimen are obviously different from those in the conventional triaxial loading test. Further, the influence factors of rock mechanical properties under unloading conditions are more complex. It is difficult to analyze the deformation characteristics of rock specimens under confining pressure unloading only by studying the deformation during unloading fracture. Therefore, the ratio of axial strain increment to confining pressure increment $\Delta\varepsilon$ and axial strain rate is introduced to analyze the influence of the unloading rate of confining pressure on the deformation characteristics of specimens.

3.2.1. Influence of unloading Rate on the Ratio of Axial Strain Increment to Confining Pressure Increment. According to Figures 5(b)–5(d), under confining pressure unloading, the initial confining pressure has a significant effect on the deformation characteristics of the specimen during the fracture process. In order to eliminate the influence of initial confining pressure on unloading deformation and accurately analyze the influence law of unloading rate on the deformation characteristics of the specimen, a new physical quantity which is the ratio of axial strain increment to confining pressure increment [32] is introduced in this study. And it is defined as follows:

$$\Delta\varepsilon = \frac{\Delta\varepsilon_1}{\Delta\sigma_3}, \tag{1}$$

where $\Delta\varepsilon_1$ is the axial strain increment caused by confining pressure unloading between the starting point of confining pressure unloading and the stress drop point; $\Delta\sigma_3$ is the decrement of confining pressure, in MPa. The ratio of axial strain increment to confining pressure increment $\Delta\varepsilon$ is a physical quantity that characterizes the speed of axial strain increment changing in unit confining pressure. It can well reflect the effect of different unloading rates on the axial deformation of the specimen and eliminate the effect of confining pressure on the axial strain. In this test, under different initial confining pressures, the relationship between the ratio of axial strain increment to confining pressure increment $\Delta\varepsilon$ and the unloading rates of confining pressure is shown in Figure 6.

According to Figure 6, the ratio of axial strain increment to confining pressure increment $\Delta\varepsilon$ decreases as the unloading rate of confining pressure increases, and the relationship between the two is significantly affected by the initial confining pressure. Specifically, when the initial confining pressure is high (20 MPa), the change trend of the ratio of axial strain increment to confining pressure increment $\Delta\varepsilon$ with the unloading rate of confining pressure is steep; however, when the initial confining pressure is relatively low (5 MPa and 10 MPa), the change trend of the ratio of axial strain increment to confining pressure increment $\Delta\varepsilon$ with the unloading rate of confining pressure is relatively gentle. When the unloading rate of confining pressure ranges from 0.002 to 0.02 MPa/s, it has a significant impact on the ratio of axial strain increment to confining pressure increment $\Delta\varepsilon$; when the unloading rate of confining pressure ranges from 0.02 to 0.2 MPa/s, the change rate of $\Delta\varepsilon$ is relatively small. Therefore, a faster unloading rate and a higher initial confining pressure can restrain the axial deformation of granite specimens. Conversely, when the unloading rate is small and the initial confining pressure is small, the ratio of axial strain increment to confining pressure increment $\Delta\varepsilon$ is relatively large, which indicates that the axial deformation of granite specimen is significantly affected by unloading, and the damage deformation of granite specimen is relatively sufficient.

3.2.2. Strain Rate Evolution of Samples under Different Unloading Rates and Confining Pressure. According to Figure 5, in the triaxial confining pressure unloading test with constant axial pressure, the peak axial strain of the specimen decreases obviously with the increase of unloading rate of confining pressure. In order to reflect the speed of axial deformation of specimens under different initial confining pressures and unloading rates, and to further study the deep-seated reasons for the above phenomenon, the axial strain rate [33] is introduced here to further analyze the deformation characteristics of specimens under different unloading rates during the whole unloading process. The axial strain rate is the axial strain increment of the specimen per unit time, which is calculated according to the following formula.

$$\dot{\varepsilon} = \frac{\varepsilon_{t+1} - \varepsilon_t}{\Delta t}. \tag{2}$$

In the formula, $\dot{\varepsilon}$ is the axial strain rate of the specimen, in s^{-1}; ε_{t+1} and ε_t are the axial strain of specimen at the time of $t + 1$ and t; Δt is the sampling interval (0.2 s), in seconds. The axial strain rate can reflect the axial deformation speed of specimens under different initial confining pressures and different unloading rates of confining pressure; the larger the axial strain rate, the larger the axial deformation per unit time.

Under different initial confining pressures, the variation characteristics of axial strain rate of granite specimen during confining pressure unloading are basically the same. In order to present the variation of strain rate with time more intuitively, we collect and study the values of strain rate for the time interval when the confining pressure is reduced by 0.04 MPa each time. When the initial confining pressure is 5 MPa and 20 MPa, the variation characteristics of axial strain rate under different unloading rates of confining pressure are shown in Figure 7.

According to Figure 7, the axial strain rate of the specimen is highly correlated with the initial confining pressure and the unloading rate of confining pressure. (1) Under the same initial confining pressure, the greater the unloading rate is, the greater the axial strain rate is. Taking the initial confining pressure of 5 MPa as an example, when the unloading rate of confining pressure is 0.002 MPa/s, the axial strain rate of the specimen is below $0.8 \times 10^{-5}\ s^{-1}$ and its peak value is $1.089 \times 10^{-5}\ s^{-1}$; when the unloading rate is 0.02 MPa/s, the axial strain rate ranges from 0.5×10^{-5} to

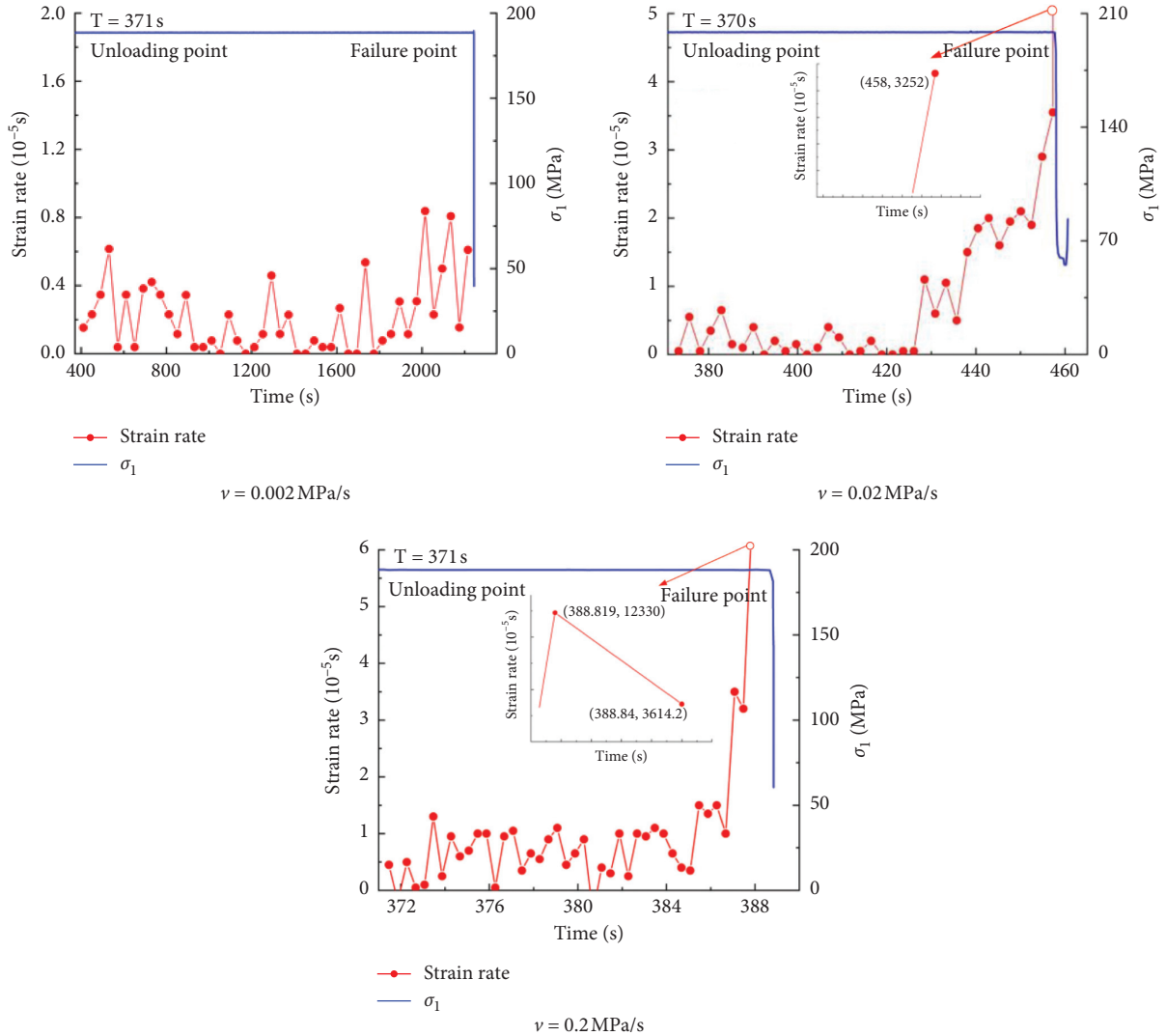

(a)

Figure 7: Continued.

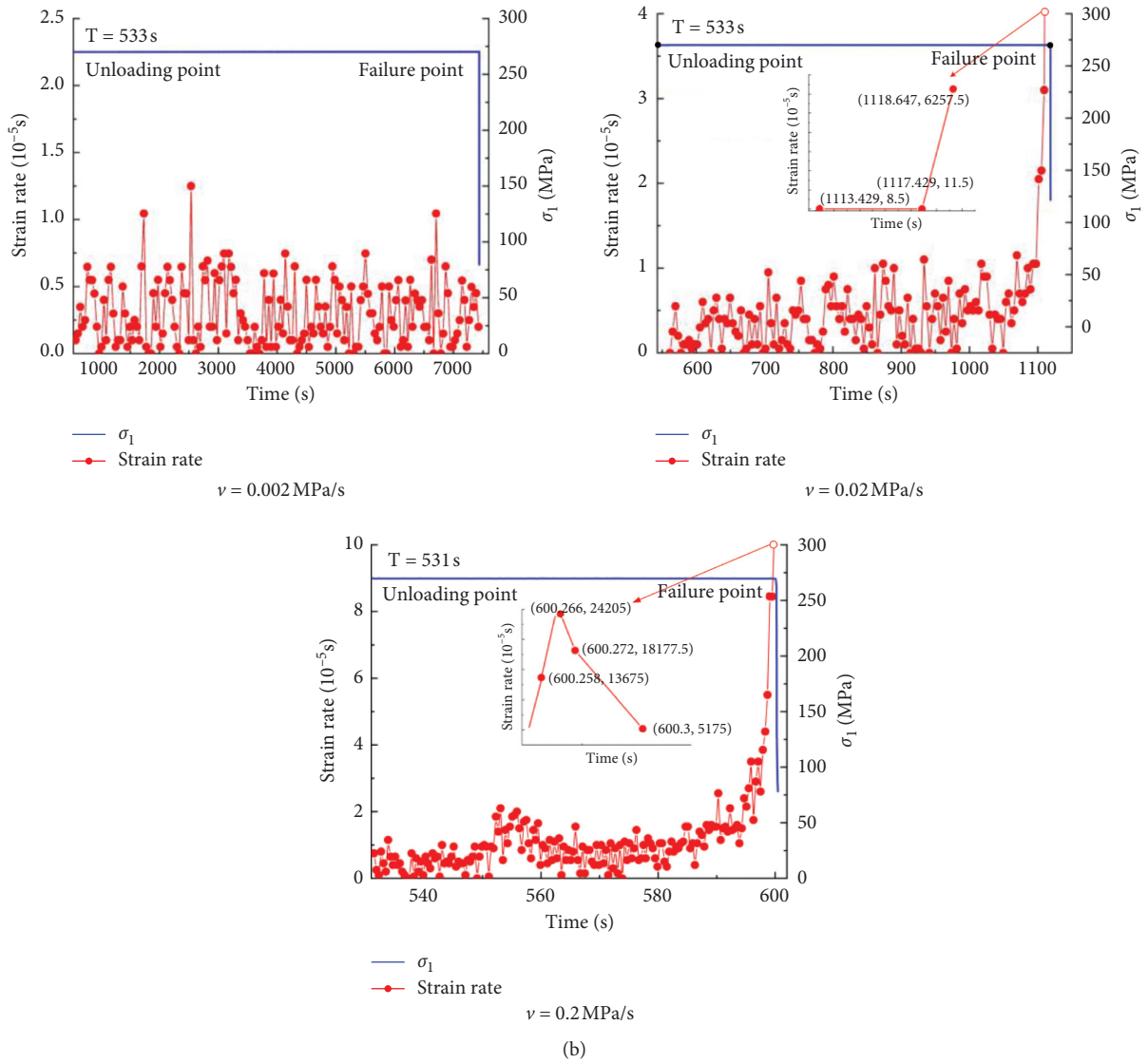

Figure 7: Variation of axial strain rate in the process of confining pressure unloading. (a) $\sigma_3 = 5$ MPa. (b) $\sigma_3 = 20$ MPa.

$1 \times 10^{-5}\ s^{-1}$ and its peak value is $0.325\ s^{-1}$; when the unloading rate is 0.2 MPa/s, the axial strain rate exceeds $1 \times 10^{-5}\ s^{-1}$ and its peak value is $1.233\ s^{-1}$. (2) Under the same unloading rate of confining pressure, the axial strain rate increases with the increase of the initial confining pressure. When the unloading rate is 0.002 MPa/s, the average axial strain rate of the specimen under the confining pressure of 5 MPa is $0.3 \times 10^{-5}\ s^{-1}$ and that under the confining pressure of 20 MPa is $0.5 \times 10^{-5}\ s^{-1}$. Notably, when the unloading rate is 0.2 MPa/s, the peak value of axial strain rate under the confining pressure of 5 MPa is $1.233\ s^{-1}$ and that under the confining pressure of 20 MPa is $2.421\ s^{-1}$. (3) Under the same unloading rate of confining pressure, the larger the initial confining pressure is, the longer the stability time of axial pressure (the time duration from the beginning of confining pressure unloading to specimen fracture) and the deformation time of specimen under confining pressure unloading will be. When the unloading rate is 0.002 MPa/s, the stability time of the specimen under the confining pressure of 5 MPa is 1876s and that under the confining pressure of 20 MPa is 6906 s. Conversely, under the same initial confining pressure, the stability time decreases rapidly with the increase of the unloading rate of confining pressure. Taking the confining pressure of 20 MPa for instance, when the unloading rate of confining pressure increases from 0.002 MPa/s to 0.2 MPa/s, the stability time decreases from 6906 s to 69 s. (4) Generally, the axial strain rate increases with time. As the unloading rate of confining pressure and initial confining pressure increases, the overall trend and peak value of the axial strain rate curve are more significant. The greater the unloading rate of confining pressure is, the more obviously the axial strain rate is affected by the unloading rate. This phenomenon is confirmed by the difference in deformation rate and deformation amount of surrounding rock caused by different excavation methods (drilling and blasting method and tunneling boring method) in underground engineering. (5) The curves of axial strain rate versus time fluctuate in different degrees at the

unloading stage, which is more obvious at low and medium unloading rates, while the fluctuation is relatively weak at a higher unloading rate. As mentioned above, with a small unloading rate of confining pressure, the stability time of axial pressure is relatively long, so that the micro cracks initiate and continue to increase and then fully develop into large-scale cracks; further, micro cracks initiate again at the tip of the original cracks. This phenomenon occurs repeatedly and alternately in the middle and early stages of the unloading process, so the fluctuation of the strain rate curve is obvious. Comparatively, when the unloading rate of confining pressure is large, the specimen does not have enough time to develop more micro cracks, and the energy is concentrated and dissipated in the larger cracks. The specimen is unloaded in a short time, so the fluctuation phenomenon is weakened.

3.3. Influence of Unloading Rate on the Strength Characteristics. With a limited number of granite specimens in this study, although we have taken corresponding measures during field sampling, the discreteness of rock specimen strength still exists. Therefore, it is difficult to guarantee the uniform initial damage degree of the specimen by loading axial pressure to 80% of the conventional triaxial compressive strength, which affects the merely study effect of unloading rate on the strength characteristics of granite specimen. To solve this issue, the normalized confining pressure decreased parameter (k) is introduced to study the strength characteristics of granite specimens under different unloading rates of confining pressure [32]. The normalized confining pressure decreased parameter k is the ratio of the unit decrement of confining pressure R to the normalized parameter U of strength dispersion degree; the strength dispersion normalized parameter U is the ratio of the conventional triaxial peak strength to the difference between the unloading initial axial pressure and the strength of stress drop. The physical quantities are defined as follows:

$$k = \frac{R}{U}, \tag{3}$$

$$R = \frac{\Delta\sigma_3}{\sigma_3^0}, \tag{4}$$

$$U = \frac{\sigma_c}{\sigma_1^0 - \sigma_{\text{unloading}}^0}. \tag{5}$$

In the formula, σ_3^0 is the preset initial confining pressure, in MPa; σ_c is the conventional triaxial compressive strength of the specimen under the preset initial confining pressure, in MPa; σ_1^0 is the preset initial axial stress, in MPa; and $\sigma_{\text{unloading}}^0$ is the axial stress at the stress drop point, in MPa. The normalized confining pressure decreased parameter k represents the decremented level of confining pressure when the specimen experiences unloading fracture under the same condition. The smaller the k is, the smaller the decrement of the confining pressure is. That is to say, in this mechanical state, with only a small amount of confining pressure loss, the specimen will experience a fracture process, which reflects the deterioration degree of rock strength due to unloading.

According to the above definition, the relationship between the normalized confining pressure decreased parameter k and the unloading rate of confining pressure in this test is shown in Figure 8.

When the unloading rate remains the same and lower than 0.0095 MPa/s, the larger the initial confining pressure is, the larger the normalized confining pressure decreased parameter is, indicating that rock strength increases with the increase of the initial confining pressure. It is the same with the results of the conventional triaxial compression test, which indicates that the main controlling factor of rock strength in this stage is the initial confining pressure. However, when the unloading rate exceeds 0.0095 MPa/s, the larger the initial confining pressure is, the smaller the normalized confining pressure decreased parameter is, indicating that the unloading damage of rock specimen in this stage is mainly affected by the unloading rate of confining pressure. From the microscopic point of view, when the unloading rate of confining pressure is small, the crack propagation of rock specimen is more sufficient, and the confining pressure has a greater impact on the crack development degree during the fracture process. However, when the unloading rate increases by a certain threshold, the stress adjustment speed of the specimen lags behind the dynamic change of the confining pressure, and the internal cracks are not fully developed when the rock is destroyed, so the unloading rate plays a dominant role in the strength of the specimen.

4. Strength Criterion for Granite and Parameter Characteristics Analysis under Confining Pressure Unloading

4.1. Strength Criterion for Granite under Confining Pressure Unloading. The Mohr–Coulomb strength criterion expressed by maximum principal stress and minimum principal stress is the most widely used strength theory in rock mechanics. This criterion characterizes the relationship between peak strength and confining pressure of rock specimens under triaxial condition, as shown in

$$\sigma_1 = \xi\sigma_3 + \sigma_c, \tag{6}$$

where σ_c is the theoretical uniaxial compressive strength of the specimen, and ξ is the influence coefficient of confining pressure on the bearing capacity of the rock specimen. In Formula (6), ξ and σ_c are the strength parameters related to cohesion and the internal friction angle of the specimen. The relationship among k, b, c, and φ is shown in

$$\xi = \frac{1 + \sin\varphi}{1 - \sin\varphi}, \tag{7}$$

$$\sigma_c = \frac{2c\cos\varphi}{1 - \sin\varphi}. \tag{8}$$

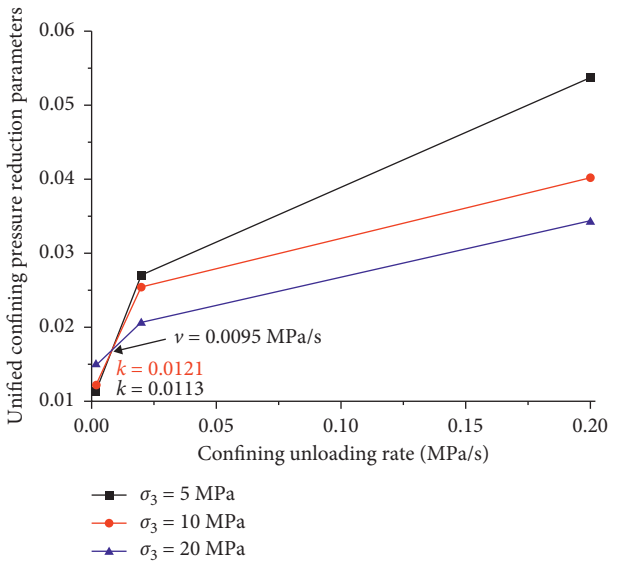

Figure 8: Unified confining pressure reduction parameters under different confining pressure unloading rates.

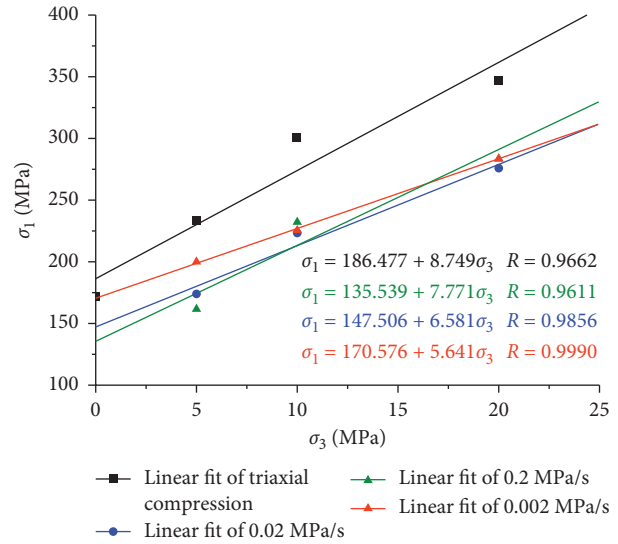

Figure 9: Mohr–Coulomb strength curves of granite.

Therefore, the relationship between triaxial compressive strength and confining pressure of the specimen can be expressed as follows:

$$\sigma_1 = \frac{1+\sin\varphi}{1-\sin\varphi}\sigma_3 + \frac{2c\cos\varphi}{1-\sin\varphi}. \tag{9}$$

Through trigonometric function conversion, the relationship between internal friction angle and cohesion of rock specimen under different unloading rates of confining pressure is obtained:

$$\varphi = \arcsin\left(\frac{\xi-1}{\xi+1}\right), \tag{10}$$

$$c = \sigma_c\frac{1-\sin\varphi}{2\cos\varphi}. \tag{11}$$

According to the above Mohr–Coulomb strength criterion, the peak strength and confining pressure of specimens under different initial confining pressures and different unloading rates of confining pressure are fitted. The fitting results are shown in Figure 9 and Table 2.

It can be seen from Figure 9 and Table 2 that the correlation coefficient *R of fitting test results based on the Mohr–Coulomb strength criterion ranges from 0.9611 to 0.9990, which* are all greater than 0.95, indicating that the Mohr–Coulomb strength criterion can better reflect and analyze the fracture strength characteristics of specimens under triaxial unloading confining pressure stress state test conditions.

4.2. Evolution Law of Deformation Parameters for Granite under Confining Pressure Unloading. According to the Mohr–Coulomb strength criterion, the parameters k and b are obtained by fitting the peak strength and confining

Table 2: Linear fitting results of two strength criteria.

Unloading rate/(MPa/s)	Fitting parameters of the Mohr–Coulomb strength criterion		
	ξ	σ_c	R
Triaxial compression	8.749	186.477	0.966
0.002	7.771	135.539	0.961
0.02	6.581	147.506	0.985
0.2	5.641	170.576	0.999

pressure of granite specimens under different initial confining pressures and different unloading rates of confining pressure (as shown in Table 2). The cohesion c and internal friction angle φ of granite specimens under different unloading rates of confining pressure can be obtained by further calculation, as shown in Table 3. From Table 3, as to make confining pressure unloading with constant axial pressure, the cohesion of granite specimen decreases with the increase of unloading rate of confining pressure. When the unloading rate increases from 0.002 MPa/s to 0.2 MPa/s, the cohesion of the specimen decreases by 30.50%. The internal friction angle increases with the increase of unloading rate of confining pressure. When the unloading rate increases from 0.002 MPa/s to 0.2 MPa/s, the internal friction angle of the specimen increases by 11.32%. The unloading rate weakens the cohesion of the granite specimen and strengthens the internal friction angle, and the weakening effect on the cohesion is stronger than the strengthening effect on the internal friction angle. The internal reasons for the above phenomenon are as follows: under the condition of low unloading rate, the opening trend of internal microcracks is weak, and the propagation mode of fracture end is mainly shear fracture. The fracture angle and internal friction angle of the specimen are relatively small, and the fracture shear-type propagation is conducive to the bond strength of the granite specimen, so the cohesion of the specimen is relatively high under a low unloading rate. When the unloading rate is high, the micro crack opening trend of

Table 3: Strength parameters of granite samples under different unloading confining pressure rates.

Confining pressure unloading rate (MPa/s)	Cohesion c (MPa)	Internal friction φ (°)
0.002	35.86	44.37
0.02	28.02	47.89
0.2	22.32	51.80

the specimen is enhanced, and the crack tip propagation mode changes from shear fracture to tensile fracture. The fracture angle of the specimen is larger, so the internal friction angle is larger and the cohesion is smaller.

In the triaxial confining pressure unloading test with constant axial pressure, the variation of cohesion and internal friction angle of granite specimen with unloading rate is shown in Figure 10.

As we can see, the cohesion and internal friction angle of granite specimen have a good logarithmic relationship with the unloading rate, with R being 0.9924 and 0.9717, respectively. With the increase of unloading rate, the decrease and increase rates of cohesion and internal friction angle decrease. In the range of relatively low unloading rate (0.002 MPa/s~0.02 MPa/s), the average decrease rate of cohesion is 347.22, and the average increase rate of internal friction angle is 112.22; in the range of relatively high unloading rate (0.02 MPa/s~0.2 MPa/s), the average decrease rate of cohesion is 24.67, and the average increase rate of internal friction angle is 17.33. It can be summarized that in the range of relatively low unloading rate, the weakening and strengthening effects of unloading rate on cohesion and internal friction angle are more obvious. With the increase of unloading rate, the weakening and strengthening effects of unloading rate on cohesion and internal friction angle gradually decline.

5. Acoustic Fracture Process Characteristic of Granite under Confining Pressure Unloading

5.1. Experiments on the Acoustic Emission Characteristics of Granite Specimens. In the process of damage evolution and energy release of rock materials, elastic waves are generated. Monitoring the release of elastic waves by acoustic emission technology can indirectly characterize the damage process of rock [34–36]. Figure 11 shows the relationship between axial stress and acoustic emission ringing count of granite specimens and time during the confining pressure unloading. The acoustic emission characteristics of specimens under different unloading rates are obtained when the initial confining pressure is 5 MPa (the acoustic emission characteristics under other test conditions are basically the same).

According to Figure 11, at the initial loading stage, the original cracks in granite specimens begin to close; during and after the crack closing process, acoustic emission (AE) events caused by occlusal fracture of some rough crack surfaces occur. However, only a small number of AE events appear at this time, and this shows fluctuation. With continuous loading, the deformation of the specimen enters the elastic stage, in which the load on the specimen is not enough to form more new micro cracks, but the acoustic emission events will occur due to the sliding of some closed cracks. With further loading, the deformation of the specimen enters the plastic stage, in which the number of new cracks inside the specimen, the damage degree, and the acoustic emission count increase obviously.

When the axial compression load reaches the predetermined load, it enters the stage of confining pressure unloading; the stress state of the specimen changes due to the change of the load application mode. During the stress adjustment process, the damage degree of the specimen further develops, and the acoustic emission begins to be active. With the further unloading of confining pressure, the damage degree of the specimen reaches a certain degree, the internal micro cracks of the specimen extend and coalesce, and the macro fracture surface is gradually formed. At this time, the acoustic emission count reaches the maximum. Subsequently, the macro fracture surface is formed, the axial stress drops rapidly, and the acoustic emission events decrease rapidly.

According to Figures 11(a) and 11(b), when the unloading rate is small, the AE count increases more evenly, and the ringing count versus time curve will appear in the active stage before and during the confining pressure unloading, notably, the AE count is obviously higher than that of a high unloading rate. The results show that the damage and deformation of the specimen develop slowly at a low unloading rate, and the AE count increases obviously. In addition, when the axial stress drops, the AE count is still high, which indicates that the brittleness of the specimen at a low unloading rate is weaker than that at a high unloading rate. According to Figure 11(c), when the unloading rate is high, the internal deformation of the specimen is not fully developed, and the sudden fracture occurs within a very short time of less than 50 s. The increasing feature of the AE count of the specimen is relatively not obvious, so the AE count increases to the maximum value instantaneously at the beginning of confining pressure unloading.

5.2. Fracture Properties of Granite under Confining Pressure Unloading. In this study, when the granite specimen is destroyed under the conventional triaxial and different unloading rates, the crack sound is heard clearly, which shows the obvious brittle fracture characteristics of the granite specimen. The photos of fracture characteristics of granite specimens under conventional triaxial compression and triaxial confining pressure unloading with constant axial pressure are shown in Figure 12.

From the macroscopic fracture surface distribution and mechanical properties, the following rules can be obtained. (1) Under the condition of conventional triaxial compression test, granite specimens show typical shear fracture characteristics, and the internal damage formed in the process of deformation and fracture is relatively concentrated, the fracture surface is

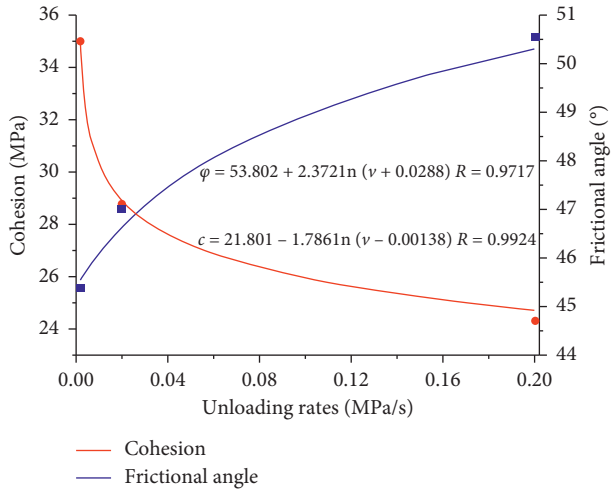

Figure 10: Cohesion and friction angle of granite under different unloading rates.

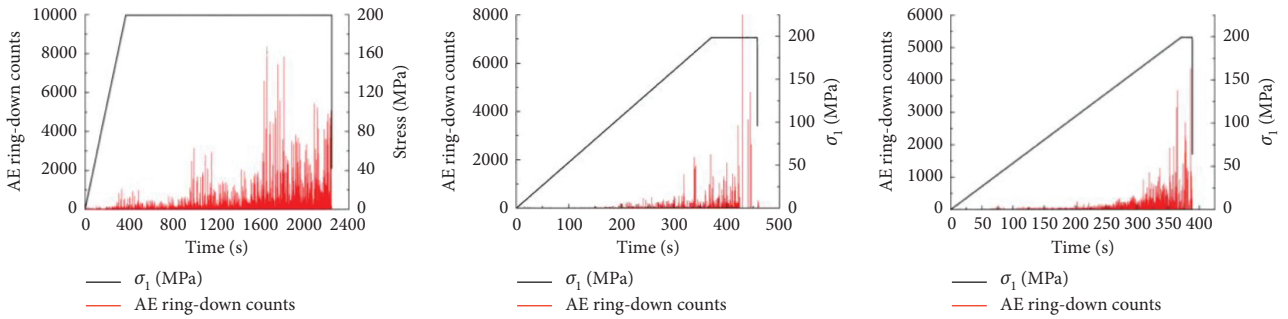

Figure 11: AE characteristics of granite under different confining pressure unloading rates. (a) $v = 0.002$ MPa/s. (b) $v = 0.02$ MPa/s. (c) $v = 0.2$ MPa/s.

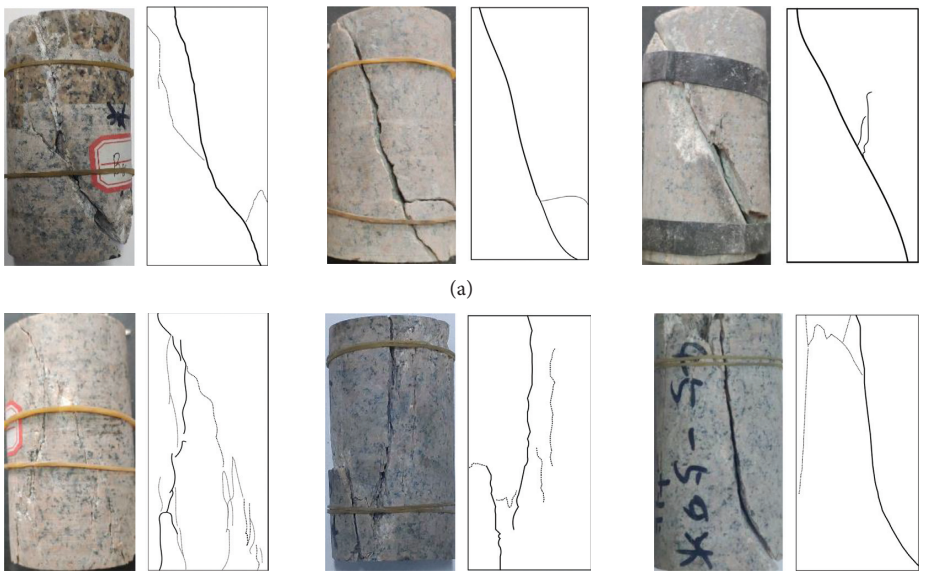

(a)

(b)

Figure 12: Continued.

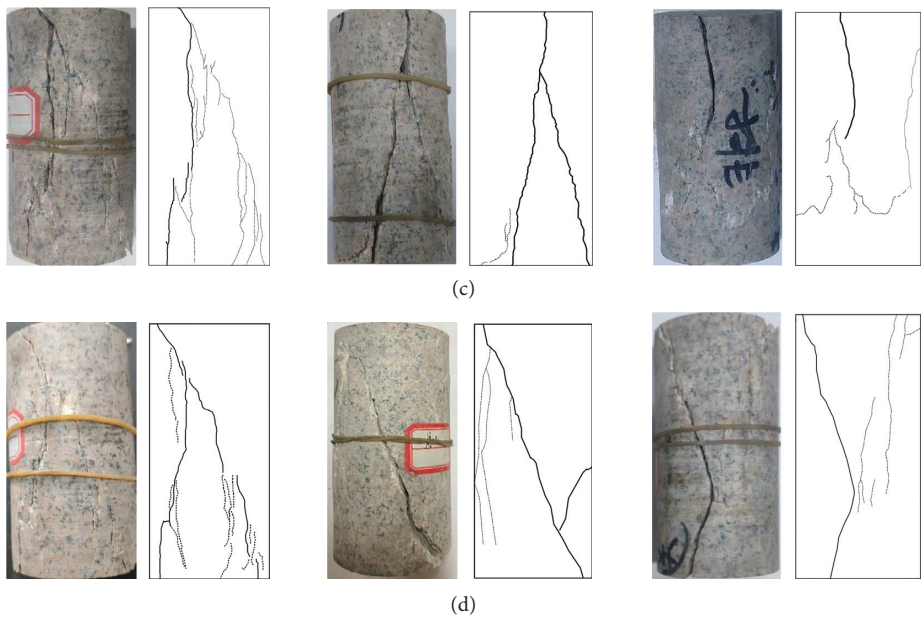

(c)

(d)

Figure 12: Photos of granite specimens' facture under unloading confining pressure and triaxial compression. (a) Triaxial compression test. (b) $v = 0.2$ MPa/s. (c) $v = 0.02$ MPa/s. (d) $v = 0.002$ MPa/s.

relatively single (as shown in Figure 12(a)), and the fracture angle ranges from 65.5° to 71.2°, which is close to the theoretical fracture angle of 71.3° predicted by the Mohr–Coulomb strength criterion ($\theta = 45° + \varphi/2$). (2) The fracture characteristics of granite specimens under triaxial constant axial pressure unloading stress path are obviously different from those under conventional triaxial stress path; under the condition of constant axial pressure confining pressure unloading test, the fracture mode of the specimen is affected by both the unloading rate and the initial confining pressure. Under different test conditions, the fracture characteristics of the specimen are significantly different. (3) When the unloading rate is the same, with high initial confining pressure, the specimens show obvious tensile fracture; with low initial confining pressure, the specimens are mainly shear or shear-tension composite fractures. When the initial confining pressure is the same, with the increase of unloading rate, the fracture characteristics of specimens show a transition from shear or shear-tension composite fracture to tensile fracture. (4) Under the same unloading rate, the unloading amplitude (initial confining pressure) and the unloading rate under the same initial confining pressure are the source power of the difference and transformation of fracture characteristics of specimens under the condition of constant axial pressure unloading confining pressure test. Further, the difference of crack initiation and propagation mode is the internal mechanism of different fracture characteristics, and the weakening/strengthening of cohesion and internal friction angle is another external manifestation.

6. Conclusions

In order to study the mechanical properties and fracture process characteristics of deeply buried granite under confining pressure unloading, a triaxial confining pressure unloading test with constant axial pressure was carried out and acoustic emission synchronous monitoring was conducted. Based on the analysis of the test results, the following conclusions are obtained:

(1) Under the condition of triaxial confining pressure unloading test with constant axial pressure, the deviatoric stress-strain curve of granite specimen can be divided into compaction stage, linear elastic deformation stage, plastic deformation stage, and fracture stage. When the unloading rate is small, the unloading platform appears in the stage before and after the peak value of the deviatoric stress-strain curve of granite specimens, and the unloading effect is obvious, with significant ductility characteristics. When the unloading rate is large, the specimen shows brittleness characteristics. The axial peak strain decreases with the increase of the unloading rate, and the axial strain rate increases with the increase of initial confining pressure and the unloading rate of confining pressure. The axial strain rate versus time curves of the specimens fluctuate in different degrees at the unloading stage, and the fluctuation is obvious at the low and medium unloading rate, while it weakens at the high unloading rate.

(2) The ratio of axial strain increment to confining pressure increment of granite specimens decreases with the increase of the unloading rate and the relationship between them is significantly affected by the initial confining pressure. The axial deformation of granite specimens is significantly affected by unloading. The faster unloading rate and higher initial confining pressure can restrain the axial deformation of granite specimens. At the same unloading rate, the larger the initial confining

pressure is, the larger the normalized confining pressure decreased parameter will be. The strength of specimens under confining pressure unloading increases with the increase of initial confining pressure. When the unloading rate is high, the stress adjustment speed of the granite specimen lags behind the dynamic change of confining pressure, and the internal cracks are not fully developed when the sample is destroyed. The unloading rate plays a dominant role in controlling the strength of granite specimens under confining pressure unloading.

(3) The Mohr–Coulomb strength criterion can reflect the strength characteristics of specimens under triaxial unloading confining pressure. The cohesion of granite specimens decreases with the increase of unloading rate, and the internal friction angle increases with the increase of unloading rate. The unloading rate weakens the cohesion of granite specimens and strengthens the internal friction angle, and the weakening effect is stronger than the strengthening effect. There is a good logarithmic relationship between the cohesion and internal friction angle of granite specimens and the unloading rate of confining pressure. With the increase of unloading rate, the decrease and increase rates of cohesion and internal friction angle decrease; at the low unloading rate, the weakening and strengthening effect of unloading rate on cohesion and internal friction angle is more obvious.

(4) When the unloading confining pressure rate is small, the acoustic emission ringing count increases more evenly, and the active stage of acoustic emission appears during the middle period before the unloading of confining pressure, the acoustic emission ringing count is obviously higher, and the deformation and damage of the specimen develop slowly. At a high unloading rate of confining pressure, the ringing count increases rapidly to the maximum value at the initial stage of confining pressure unloading, and the specimen suddenly fails in a very short time. The results show that the fracture mode of specimens is affected by both the unloading rate and the initial confining pressure. At the same unloading rate, the specimens with high initial confining pressure exhibit obvious tensile fracture, while the specimens with low initial confining pressure exhibit shear fracture or shear-tension composite fracture; when the initial confining pressure is the same, with the increase of unloading rate, the fracture characteristics of specimens show the transition from shear or shear-tension composite fracture to tensile fracture.

Data Availability

The data used to support the findings of this study are available from the corresponding author upon request.

Conflicts of Interest

The authors declare that there are no conflicts of interest regarding the publication of this paper.

Acknowledgments

This research was funded by the National Natural Science Foundation of China (51778215), China Postdoctoral Science Foundation Funded Project (no. 2018M631114), and Henan Province Science Foundation for Youths Project (no. 212300410146). The authors greatly appreciate the financial supports from funding bodies.

References

[1] B. P. Simser, "Rockburst management in Canadian hard rock mines," *Journal of Rock Mechanics and Geotechnical Engineering*, vol. 11, no. 5, pp. 1036–1043, 2019.

[2] F. Ren, Y. Chang, and M. He, "A systematic analysis method for rock failure mechanism under stress unloading conditions: a case of rock burst," *Environmental Earth Sciences*, vol. 79, no. 15, p. 370, 2020.

[3] K. Duan, Y. Ji, W. Wu, and C. Y. Kwok, "Unloading-induced failure of brittle rock and implications for excavation-induced strain burst," *Tunnelling and Underground Space Technology*, vol. 84, pp. 495–506, 2019.

[4] Y. Zong, L. Han, J. Wei, and S. Wen, "Mechanical and damage evolution properties of sandstone under triaxial compression," *International Journal of Mining Science and Technology*, vol. 26, no. 4, pp. 601–607, 2016.

[5] Y. Zhang, Y. Yang, and D. Ma, "Mechanical characteristics of coal samples under triaxial unloading pressure with different test paths," *Shock and Vibration*, vol. 2020, Article ID 8870821, 10 pages, 2020.

[6] J.-J. Wang, M.-N. Liu, F.-X. Jian, and H.-J. Chai, "Mechanical behaviors of a sandstone and mudstone under loading and unloading conditions," *Environmental Earth Sciences*, vol. 78, no. 1, p. 30, 2019.

[7] T. Qin, Y. Duan, H. Sun, H. Liu, and W. Lei, "Energy evolution and acoustic emission characteristics of sandstone specimens under unloading confining pressure," *Shock and Vibration*, vol. 2019, Article ID 1612576, 9 pages, 2019.

[8] Y. Liang, Q. Li, Y. Gu, and Q. Zou, "Mechanical and acoustic emission characteristics of rock: effect of loading and unloading confining pressure at the postpeak stage," *Journal of Natural Gas Science and Engineering*, vol. 44, pp. 54–64, 2017.

[9] X. Li, H. Zhao, B. Wang, and T. Xiao, "Mechanical properties of deep-buried marble material under loading and unloading tests," *Journal of Wuhan University of Technology-Mater Science Education*, vol. 28, no. 3, pp. 514–520, 2013.

[10] H. Q. Xie and C. H. He, "Study of the unloading characteristics of a rock mass using the triaxial test and damage mechanics," *International Journal of Rock Mechanics and Mining Sciences*, vol. 41, pp. 74–80, 2004.

[11] J. Li, R. Wang, Y. Jiang et al., "Experimental study of sandstone mechanical properties by unloading triaxial tests," *Chinese Journal of Rock Mechanics and Engineering*, vol. 29, no. 10, pp. 2034–2041, 2010.

[12] H. Li, C. Xia, Z. Yan, K. Jiang, and L. Yang, "Study on marble unloading mechanical properties of Jinping hydropower station under high geostress conditions," *Chinese Journal of*

Rock Mechanics and Engineering, vol. 26, no. 10, pp. 2104–2109, 2007.

[13] F. Gao, K.-P. Zhou, X.-W. Luo, and J.-B. Zhai, "Effect of induction unloading on weakening of rock mechanics properties," *Transactions of Nonferrous Metals Society of China*, vol. 22, no. 2, pp. 419–424, 2012.

[14] R. Q. Huang and D. Huang, "Evolution of rock cracks under unloading condition," *Rock Mechanics and Rock Engineering*, vol. 47, no. 2, pp. 453–466, 2014.

[15] X. Si and F. Gong, "Strength-weakening effect and shear-tension failure mode transformation mechanism of rockburst for fine-grained granite under triaxial unloading compression," *International Journal of Rock Mechanics and Mining Sciences*, vol. 131, Article ID 104347, 2020.

[16] K. Zhang, H. Zhou, P. A. N. Peng-zhi et al., "Characteristics of strength of rocks under different unloading rates," *Rock and Soil Mechanics*, vol. 31, no. 7, pp. 2072–2078, 2010.

[17] L. Zhang, S. Gao, Z. Wang, and M. Ren, "Analysis on deformation characteristics and energy dissipation of marble under different unloading rates," *Tehnicki Vjesnik-Technical Gazette*, vol. 21, no. 5, pp. 987–993, 2014.

[18] D. Huang and Y. Li, "Conversion of strain energy in triaxial unloading tests on marble," *International Journal of Rock Mechanics and Mining Sciences*, vol. 66, pp. 160–168, 2014.

[19] S. Qiu, X. Feng, C. Zhang, H. Zhou, and F. Sun, Experimental research on mechanical properties of deep-buried marble under different unloading rates of confining pressures," *Chinese Journal of Rock Mechanics and Engineering*, vol. 29, no. 9, pp. 1807–1817, 2010.

[20] S.-L. Qiu, X.-T. Feng, J.-Q. Xiao, and C.-Q. Zhang, "An experimental study on the pre-peak unloading damage evolution of marble," *Rock Mechanics and Rock Engineering*, vol. 47, no. 2, pp. 401–419, 2014.

[21] R. Huang and D. Huang, "Experimental research on mechanical properties of granites under unloading condition," *Chinese Journal of Rock Mechanics and Engineering*, vol. 29, no. 1, pp. 21–33, 2010.

[22] B. Dai, G. Zhao, L. Dong, and C. Yang, "Mechanical characteristics for rocks under different paths and unloading rates under confining pressures," *Shock and Vibration*, vol. 2015, Article ID 578748, 8 pages, 2015.

[23] Y. Wang, H. Jiao, L. I. Zhen et al., "Strength and damage fracture characteristics of white sandstone under unloading confining pressure," *Journal of China Coal Society*, vol. 45, no. 8, 2020.

[24] P. Kang, L. Zhaopeng, Z. Quanle, Z. Zhenyu, and Z. Jiaqi, "Static and dynamic mechanical properties of granite from various burial depths," *Rock Mechanics and Rock Engineering*, vol. 52, no. 10, pp. 3545–3566, 2019.

[25] J. Li, F. Lin, H. Liu, and Z. Zhang, "Triaxial experimental study on changes in the mechanical properties of rocks under different rates of confining pressures unloading," *Soil Mechanics and Foundation Engineering*, vol. 56, no. 4, pp. 246–252, 2019.

[26] Y. Chen, J. Zuo, Z. Li, and R. Dou, "Experimental investigation on the crack propagation behaviors of sandstone under different loading and unloading conditions," *International Journal of Rock Mechanics And Mining Sciences*, vol. 130, Article ID 104310, 2020.

[27] X. Chen, C.-A. Tang, J. Yu, J.-F. Zhou, and Y.-Y. Cai, "Experimental investigation on deformation characteristics and permeability evolution of rock under confining pressure unloading conditions," *Journal of Central South University*, vol. 25, no. 8, pp. 1987–2001, 2018.

[28] H. A. O. Xianjie, W. E. I. Yingnan, and Y. A. N. G. Ke, "Anisotropy of crack initiation strength and damage strength of coal reservoirs," *Petroleum Exploration and Development*, vol. 48, no. 1, pp. 243–255, 2021.

[29] J. Chen, D. Jiang, S. Ren, and C. Yang, "Comparison of the characteristics of rock salt exposed to loading and unloading of confining pressures," *Acta Geotechnica*, vol. 11, no. 1, pp. 221–230, 2016.

[30] X. Li, W. Cao, Z. Zhou, and Y. Zou, "Influence of stress path on excavation unloading response," *Tunnelling and Underground Space Technology*, vol. 42, pp. 237–246, 2014.

[31] X. Hao, W. Du, Y. Zhao et al., "Dynamic tensile behaviour and crack propagation of coal under coupled static-dynamic loading," *International Journal of Mining Science and Technology*, vol. 30, no. 5, pp. 659–668, 2020.

[32] S. Qiu, X. Feng, C. Zhang, and J. Yang, "Experimental research on mechanical properties of deep marble under different initial damage levels and unloading paths," *Chinese Journal of Rock Mechanics and Engineering*, vol. 31, no. 8, pp. 1686–1697, 2012.

[33] G. Hou, J. Liang, T. Hu et al., "Effects of the unloading rate on the deformation and damage of the surrounding rock under different confining pressures," *Chinese Journal of Rock Mechanics and Engineering*, vol. 38, no. 3, pp. 433–444, 2019.

[34] L. Zhang, M. Ren, S. Ma et al., "Acoustic emission and fractal characteristics of marble during unloading fracture process," *Chinese Journal of Rock Mechanics and Engineering*, vol. 34, no. S1, pp. 2862–2867, 2015.

[35] A. Ting, Z. Ru, L. Jianfeng, and R. Li, "Space-time evolution rules of acoustic emission location of unloaded coal sample at different loading rates," *International Journal of Mining Science and Technology*, vol. 22, no. 6, pp. 847–854, 2012.

[36] Q. Meng, M. Zhang, L. Han, H. Pu, and Y. Chen, "Acoustic emission characteristics of red sandstone specimens under uniaxial cyclic loading and unloading compression," *Rock Mechanics and Rock Engineering*, vol. 51, no. 4, pp. 969–988, 2018.